Artifact Mitigation in High Energy CT via Monte Carlo Simulation

Xuemin Jin and Robert Y. Levine
Spectral Sciences, Inc., USA

Abstract— The high energy (< 15 MeV) incident polychromatic γ-ray spectrum and energy-resolved photon attenuations in steel, obtained via EGS/BEAM Monte Carlo, were applied to derive beam hardening correction in steel cylinders and pipes. Monte Carlo simulated pencil beam projections were processed using latch bit filters to isolate exiting primary photons. The beam hardening correction was applied to these projections, which were then interpolated to a uniform grid. Filtered back projections of the raysums with and without the beam hardening correction were compared. It was demonstrated that beam hardening artifacts can be successfully removed for steel structures.

1. INTRODUCTION

CT artifacts resulting from preferential absorption of lower energy photons in a polychromatic beam are known as beam hardening effects, and have been a focus of intense research [1, 2]. The beam hardening correction (BHC) involves a renormalization of each measured intensity with a correction factor that depends on the measured intensity, the polychromatic input spectrum, an energy-dependent attenuation, and a reference monoenergetic photon beam energy [1]. Steel is a high-Z dense material upon which accelerator-based high energy (> 1 MeV) photon sources are applied for nondestructive testing (NDT) CT [3]. In this paper, we apply the Monte Carlo simulated incident polychromatic γ-ray spectrum and the energy-resolved attenuation [3] to compute the BHC, and demonstrate procedures necessary to obtain corrected images with steel cylinders and pipes. Cylinders will have more beam hardening and scattering disparity along a projection, whereas the thin pipe boundaries are more easily masked by artifacts.

2. BEAM HARDENING CORRECTION OVERVIEW

Formally, the measured raysum, r_0, from a polychromatic source with normalized incident spectral density $S_n(E)$ through a homogeneous material of attenuation $\mu(E)$ and thickness d is modeled as

$$r_0 = -\ln\left[\int S_n(E)e^{-\mu(E)d}dE\right] \tag{1}$$

The BHC in CT converts r_0 to an equivalent raysum $\mu(E_0)d$ for a monoenergetic source of reference energy E_0 [1]. For N_0 incident photons and N detector particle counts, the raysum estimate r_0 results from $\ln(N_0/N)$. The appropriate BHC for this measurement converts r_0 to

$$r = \ln(N_0/N) + \mu(E_0)d + \ln\left[\int S_n(E)e^{-\mu(E)d}dE\right]. \tag{2}$$

Monte Carlo simulation has a significant role in determining the BHC via calculation of the input attenuation $\mu(E)$ and spectral density $S_n(E)$ in Eq. (2).

2.1. Polychromatic Sources

The accelerator that creates a breamsstrahlung-generated photon flux for high-Z NDT is similar to a radiotherapy medical accelerator, except the flattening filter and ion chamber have been removed to increase photon yields. In the accelerator head a 15 MeV electron beam is incident on a 1 cm thick tungsten slab to create bremsstrahlung photons with a continuous spectrum in the range 0–15 MeV. Primary photon fluence is defined as γ-rays created via target bremsstrahlung that do not interact anywhere further in the beam line to the scoring plane.

Monte Carlo simulations were performed for 100 million input 15 MeV electrons and simulated interactions, trajectories, and particle showers using the EGS/BEAM code [4] with 20 processors on a Beowulf cluster. A scoring plane was placed at the end of the accelerator head to compute the

~ 2 GB phase space file for the emerging 18° beam. The spectral density of the phase space particles in the central 1 cm of the beam, an area that defines a pencil beam for raysum measurements, was calculated. Figure 1 shows the spectral density for the pencil beam in which the primary photon spectrum is separated from electrons and positrons. There are energy cutoffs for photon (10 keV) and electron (0.7 MeV) transport which force the spectrum to zero. The cutoffs are chosen based on the extremely short range of these particles in solids in order to speed-up the Monte Carlo simulation [4]. The charged particle cutoff is higher, but as can be seen in Figure 1, represents a very small percentage of the particles in the beam (and also would not have a significant range in steel). In order to compute the BHC in Eq. (2) an explicit expression for the normalized spectrum $S_n(E)$ is required, which was obtained from a six order polynomial fit to the spectrum shown in Figure 1.

2.2. Steel Spectral Attenuation

The energy-resolved steel spectral attenuation, $\mu(E)$, is also employed in Eq. (2). This was derived using a series of EGS/BEAM Monte Carlo slab simulations with incident monoenergetic photons. Figure 2 contains the resulting primary photon attenuation $\mu(E)$ for steel, which is appropriate if scatter has been removed via collimation. Also shown is a third order exponential fit to the data that is applied to the BHC calculation in Eq. (2).

2.3. BHC Estimation

The steel BHC versus thickness d is derived from the following equation

$$\mathrm{BHC}(d) = \mu(5.6\,\mathrm{MeV})d + \ln\left[\int S_n(E)e^{-\mu(E)d}dE\right], \tag{3}$$

where $S_n(E)$ and $\mu(E)$ are given in Figures 1 and 2. The reference energy $E_0 = 5.6$ MeV is somewhat arbitrary. Procedures for choosing E_0 are discussed in the literature [1]. Figure 3 shows the resulting steel BHC and an exponential fit to the function BHC(d), which is used for the applications to tomographic reconstructions in the next section.

3. APPLICATION OF BHC TO TOMOGRAPHIC RECONSTRUCTION

In this section we apply the steel BHC in Figure 3 to tomographic reconstruction of steel cylinders and pipes. In order to obtain the necessary projection data via Monte Carlo simulation, we use a polychromatic photon pencil beam with the spectrum in Figure 1. The incident pencil beam had square areal dimensions with $\Delta x = \Delta y = 0.01$ cm half maxima. Projection data was obtained through a series of EGS/BEAM simulations with different incident offsets on the steel target. A scoring plane was placed behind a 19 cm lead collimator nearly two meters downstream from the steel targets. Latch bits were set to distinguish primary and scattered particles.

The specific steps in generating projection data, applying the BHC, and performing CT reconstructions were as follows: 1) obtain projection data via independent multiple-offset pencil beam

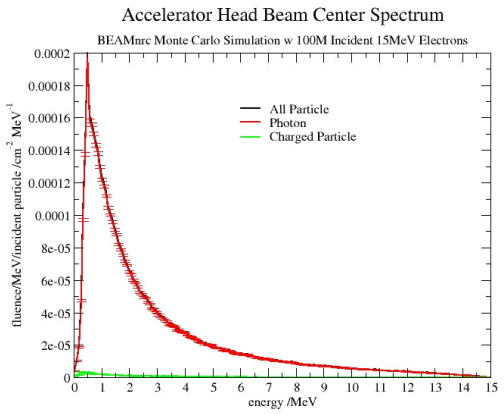

Figure 1: EGS/BEAM Monte Carlo simulation of 15 MeV accelerator head pencil beam spectral densities.

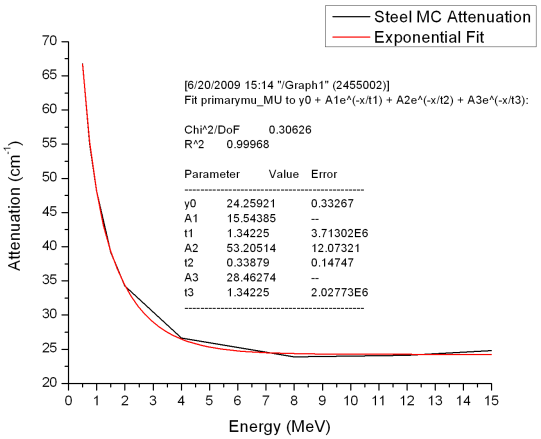

Figure 2: Steel spectral attenuation in the range 0.5–15 MeV via EGS/BEAM Monte Carlo slab calculations.

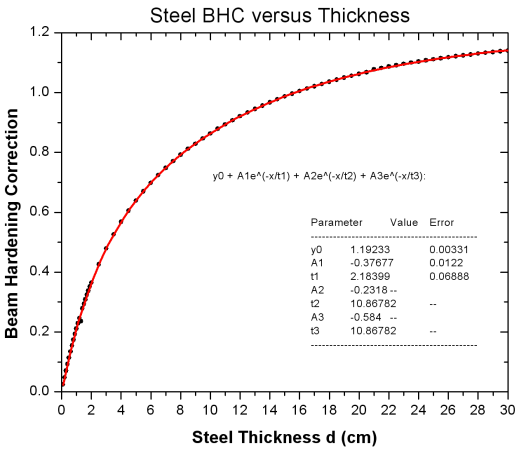

Figure 3: Steel BHC versus thickness.

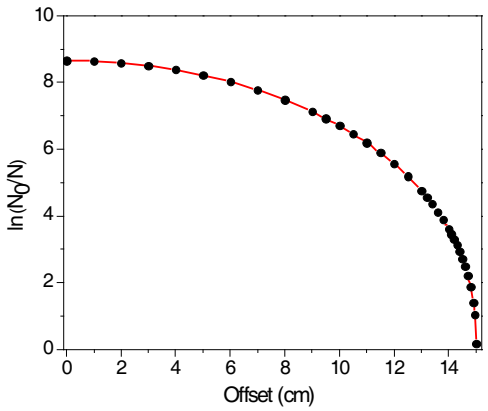

Figure 4: Projection from EGS/BEAM simulations on steel cylinder with radius of 15 cm.

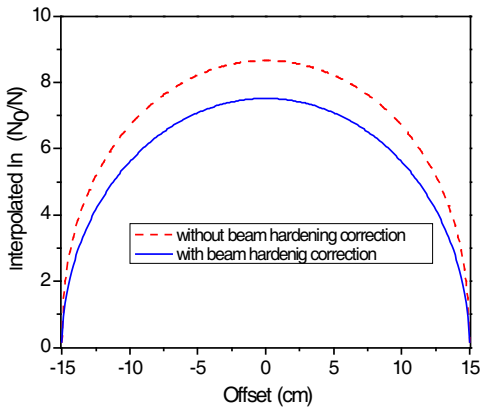

Figure 5: Interpolation of projection data to uniform 256 point grid with and without the steel BHC.

simulations using the phantom model, 2) apply spline interpolation of projection data onto an equally spaced 256 sample grid to create a 256×256 reconstructed image, and 3) perform filtered back projection using the Siddon algorithm [5] with 180 one-degree separated beams for the uncorrected reconstruction. Alternatively, after step 2, we apply the BHC in Eq. (3) to projection data, and perform the same filtered back projection reconstruction to the BHC-processed projections to obtain corrected reconstructions. The results of these procedures for the steel cylinder and pipe are shown in the following sections.

3.1. Steel Cylinder

The steel cylinder of 15 cm radius was constructed as an EGS/BEAM Monte Carlo phantom. For each offset $0.01 \times 0.01\,\mathrm{cm}^2$ pencil beam, a total of $N_0 = 200$ million incident photons were chosen from the polychromatic spectrum in Figure 1. The offsets of the incident pencil beams in centimeters for the EGS/BEAM simulations were 0, 1, 2, 3, 4, 5, 6, 7, 8, 9, 10, 10.5, 11, 11.5, 12, 12.5, 13, 13.2, 13.4, 13.6, 13.8, 14, 14.1, 14.2, 14.3, 14.4, 14.5, 14.6, 14.7, 14.8, 14.9, 14.95, 15. In order to isolate beam hardening from scatter effects, latch bits were employed to count primary photons [4]. This count of exiting photons N at the scoring plane was obtained for each pencil beam. Figure 4 shows the count plotted as $\ln(N_0/N)$ versus offset that defines the projection data. The interpolation of this function to a uniform grid is shown in Figure 5 with and without the application of the BHC in Eq. (3) using the appropriate thickness d of the steel cylinder at the corresponding offset. The magnitude of the BHC is significant, nearly a factor of 7.4 at the center of the cylinder. The filtered back projection reconstructions are shown in Figures 6 and 7. The beam hardening artifact is prominent in Figure 6(a), and is completely removed in Figure 6(b) after the application of BHC. This is further illustrated in Figure 7 with a horizontal slice through the reconstructed images in Figure 6.

3.2. Steel Pipe

The second example we considered was a steel pipe of 13 cm inner radius and 15 cm outer radius. In order to boost photon yields and isolate beam hardening effects, the pipe phantom was set in a vacuum. Consequently, only $N_0 = 5$ million photons were needed for each pencil beam simulation. This allowed dense beam offset sampling near the inner and outer edges of the pipe. The offsets

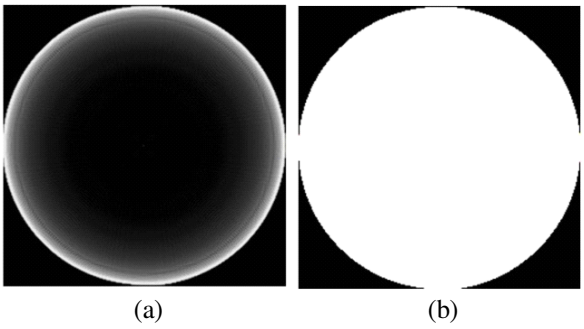

Figure 6: Tomographic reconstructions of steel cylinder from EGS/BEAM simulated projection in (a) without the BHC and (b) with the BHC.

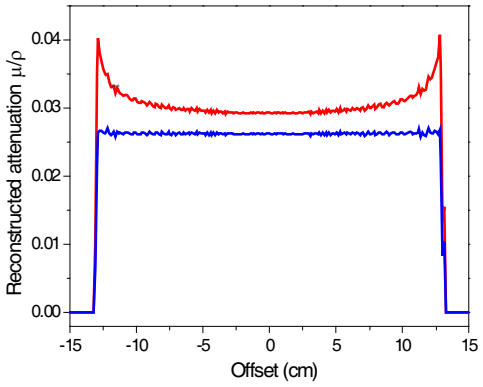

Figure 7: The red curve is from Figure 6(a) (without BHC) and the blue curve is from Figure 6(b) (with BHC).

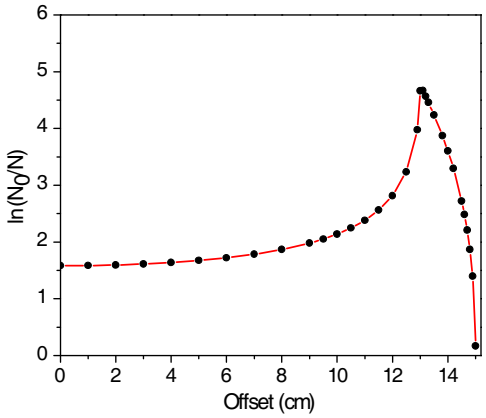

Figure 8: Primary photon fluence projection from EGS/BEAM simulations on steel pipe of inner radius 13 cm and outer radius 15 cm.

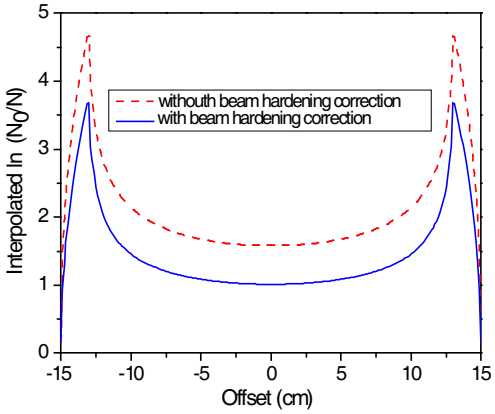

Figure 9: Projections interpolated onto equally spaced grid of 256 samples with and without the steel BHC.

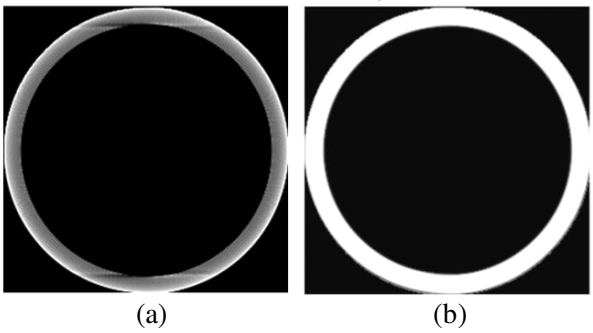

Figure 10: Tomographic reconstructions of steel pipe from EGS/BEAM projections.

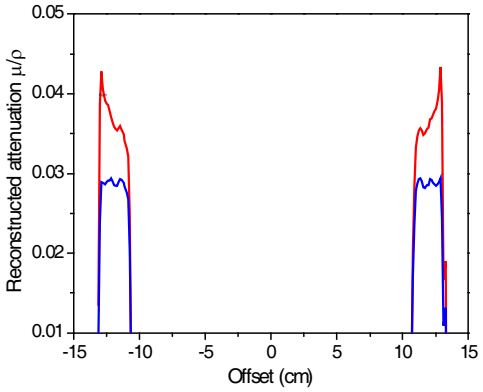

Figure 11: Horizontal slices through the reconstructions in Figure 10. The red curve is from Figure 10(a) (without BHC) and the blue curve is from Figure 10(b) (with BHC).

in centimeters were given by 0, 1, 2, 3, 4, 5, 6, 7, 8, 9, 9.5, 10, 10.5, 11, 11.5, 12, 12.5, 12.9, 13, 13.1, 13.2, 13.3, 13.5, 13.8, 14, 14.2, 14.5, 14.6, 14.7, 14.8, 14.9, and 15. We computed primary photon numbers at the scoring plane using appropriate latch bit filters. The resulting function $\ln(N_0/N)$ versus offset is plotted in Figure 8. Spline interpolation to a uniform grid was applied to the projection data, and the BHC in Eq. (2) was implemented for steel thickness d at the corresponding offset. The results shown in Figure 9 indicate a large correction in the pipe center and at the rim where the reconstruction is most delicate.

Filtered back projection reconstructions from 180 one-degree views with the raysum estimates in Figure 9 are shown in Figure 10. The beam hardening artifact is apparent in Figure 10(a) and completely removed via the (Eq. (3)) BHC application in Figure 10(b). Figure 11 shows horizontal slices through the reconstructions in Figure 10 without (red) and with (blue) the BHC. Beam hardening is observed in the cupped signature towards the edge of the pipe image.

4. CONCLUSIONS

The key inputs to high energy ($> 1\,\text{MeV}$) beam hardening correction for nondestructive testing, incident photon spectral density and material spectral attenuation, were derived via first-principles Monte Carlo simulation. In this paper, the Monte Carlo-derived BHC was shown to remove beam hardening effects for steel cylinders and pipes. The overall reconstruction corrections were remarkably successful, but required dense edge sampling and interpolation via pencil beams. These may not be available in CT measurements and processing. Nevertheless, if there is prior knowledge of the accelerator head configuration and expected materials, it is possible to derive spectra from Monte Carlo simulation for BHC calculation. In our future research, we will fully simulate the BHC procedure by including simulated calibration curves that correlate the BHC factor with measured particle counts at the detector.

REFERENCES

1. Kak, A. C. and M. Slaney, *Principles of Computerized Tomographic Imaging*, IEEE Press, New York, 1988.
2. Gao, H., L.Zhang, Z. Chen, Y. Xing, and S. Li, "Beam hardening correction for middle-energy industrial computerized tomography," *IEEE Trans. Nuclear Science*, Vol. 53, 2796–2807, 2006.
3. Jin, X., R. Y. Levine, and D. Reiss, "Spectral feature of high energy photon scatter in high-Z materials," *IEEE Trans. Nucl. Sci.*, 2011 (submitted for publication).
4. Rogers, D. W. O., B. A. Faddegon, G. X. Ding, C.-M. Ma, J. We, and T. R. Mackie, "BEAM: A Monte Carlo code to simulate radiotherapy treatment units," *Med. Phys.*, Vol. 22, 503–524, 1995.
5. Siddon, R. L., "Fast calculation of exact radiological path for a three-dimensional CT array," *Med. Phys.*, Vol. 12, 252–255, 1985.